

Watching a Protein as it Functions with 150-ps Time-Resolved X-ray Crystallography

Friedrich Schotte,¹ Manho Lim,² Timothy A. Jackson,³ Aleksandr V. Smirnov,¹ Jayashree Soman,⁴ John S. Olson,⁴ George N. Phillips Jr.,⁵ Michael Wulff,⁶ Philip A. Anfinrud¹

We report picosecond time-resolved x-ray diffraction from the myoglobin (Mb) mutant in which Leu²⁹ is replaced by Phe (L29F mutant). The frame-by-frame structural evolution, resolved to 1.8 angstroms, allows one to literally “watch” the protein as it executes its function. Time-resolved mid-infrared spectroscopy of flash-photolyzed L29F MbCO revealed a short-lived CO intermediate whose 140-ps lifetime is shorter than that found in wild-type protein by a factor of 1000. The electron density maps of the protein unveil transient conformational changes far more dramatic than the structural differences between the carboxy and deoxy states and depict the correlated side-chain motion responsible for rapidly sweeping CO away from its primary docking site.

To gain insight into the function of enzymes, much effort has gone into the determination of their three-dimensional structures (*1*). However, enzymes are dynamic molecules whose mechanistic description also requires information about intermediates along the reaction pathway. We have developed the method of picosecond x-ray crystallography and used this technique to characterize the structure of the L29F mutant of myoglobin as it evolves from the carboxy to the deoxy state. We chose this model system because transient infrared (IR) spectra of photolyzed

L29F MbCO revealed a short-lived intermediate along the ligand escape pathway. Its 140-ps lifetime is comparable to the current time resolution of macromolecular x-ray crystallography and thereby provides a stringent test of its capabilities. The time-resolved “snapshots” of this mutant’s crystal structure capture a “transition state” whose highly strained side chains apparently sweep CO away from its primary docking site in less than a nanosecond.

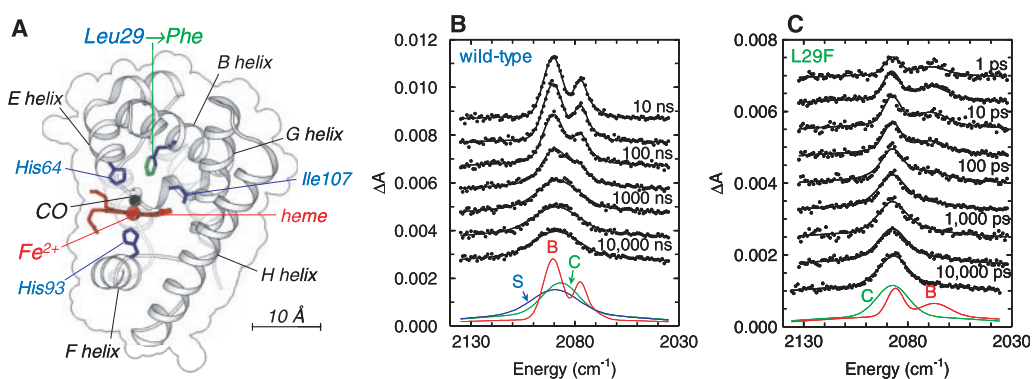
Myoglobin is an oxygen-binding heme protein (Fig. 1A) found in muscle that has long served as a model system for investigating the dynamics of ligand binding (*2*) and conformational relaxation in proteins (*3, 4*). With the heme in its chemically reduced (Fe II) ferrous state, Mb reversibly binds O₂, as well as other physiological ligands such as CO and NO. Of the three adducts, MbCO is most stable and most easily photolyzed (*5*), which makes it an ideal model for time-resolved studies. Time-resolved IR investiga-

tions of photolyzed wild-type MbCO showed that CO becomes temporarily trapped in a nearby ligand-docking site before escaping into the surrounding solvent (*6*). This site presumably mediates the transport of ligands to and from the active binding site. Molecular dynamics simulations suggested a location for this docking site (*7*), which was found to be consistent with low-temperature crystal structures of photolyzed MbCO (*8, 9*) where “docked” CO was displaced about 2 Å from the active binding site. The docking site is fashioned by the heme and amino acid side chains valine (Val⁶⁸), isoleucine (Ile¹⁰⁷), and leucine (Leu²⁹), all of which are highly conserved in mammalian Mb. Therefore, site-directed mutagenesis at these sites would likely influence the function of the protein. Indeed, in the L29F mutant (where Leu²⁹ is replaced by phenylalanine), the O₂ affinity is elevated by an order of magnitude, and the autooxidation rate is lowered by a comparable amount (*10*).

We determined the dynamics of ligand translocation in wild-type and L29F MbCO using femtosecond time-resolved mid-IR spectroscopy (*11*). Briefly, the samples were photolyzed by an orange laser flash, after which a time-delayed IR pulse probed the CO stretch band around 4.8 μm. The transient IR absorbance spectra of photodetached CO (Fig. 1, B and C) reveal two promptly appearing bands that are interpreted as CO at opposite orientations within the primary docking site (*6*). The two bands in wild-type Mb persist for a few hundred nanoseconds, whereas those in the L29F mutant evolve into a single, broad band within a few hundred picoseconds. The disappearance of the two bands corresponds to escape of CO from the nearby primary docking site to other locations within the protein, with the translocation being faster in the L29F mutant than in wild-type Mb by a factor of 1000.

¹Laboratory of Chemical Physics, National Institute of Diabetes and Digestive and Kidney Diseases, National Institutes of Health, Bethesda, MD 20892, USA. ²Department of Chemistry, Pusan National University, Pusan, 609-735, Korea. ³Harvard Medical School, Boston, MA 02115, USA. ⁴Department of Biochemistry and Cell Biology, Rice University, Houston, TX 77251-1892, USA. ⁵Biochemistry Department, University of Wisconsin, Madison, WI 53706, USA. ⁶European Synchrotron Radiation Facility, BP 220, 38043 Grenoble Cedex, France.

Fig. 1. Structure and time-resolved mid-IR spectra of wild-type and L29F MbCO. **(A)** The 29 position side chains for both wild-type (leucine, blue) and L29F Mb (phenylalanine, green) are shown. The heme and key nearby residues are modeled as sticks, the iron and CO as space filling spheres, and the protein as ribbon with its space-filling volume outlined. **(B and C)** The mid-IR spectral evolution, offset for clarity, is well described by consecutive equilibria ($A \leftrightarrow B \leftrightarrow C \leftrightarrow S$), where A corresponds to the CO-bound form (MbCO), B corresponds to CO trapped in a primary docking site (Mb·CO), C corresponds to CO elsewhere inside the protein (Mb·CO), and S corresponds to CO in the surrounding solvent (Mb + CO_{aq}). All rate coefficients were treated as time-independent, except $k_{A \rightarrow B}$ in wild type, which changes because of protein conformational relaxation on the same time scale as ligand escape. The



least-squares determination of the time constant for *B*-state escape was found to be 190 ns and 140 ps for wild-type and L29F Mb, respectively (measured at 10°C). For clarity, sub-nanosecond spectra of wild-type Mb are not shown. [Fig. 1A was generated with BobScript 2.5, author R. Esnouf.]

To determine three-dimensional time-resolved electron density maps of photolyzed L29F MbCO, we used picosecond Laue crystallography at the European Synchrotron and Radiation Facility (ESRF) (11). Briefly, the protein crystal was photolyzed with an orange laser flash, after which a time-delayed x-ray pulse was scattered by the sample, and its diffraction pattern was recorded (Fig. 2). Crucial to these experiments is the ability to isolate a single x-ray pulse from the synchrotron pulse train. When operated in the so-called "single-bunch" mode (implemented at the ESRF for 12 days in 2002), the time spacing between x-ray pulses is sufficient to isolate a single, intense x-ray pulse with a high-speed chopper.

The diffraction image presented in Fig. 3 contains about 3000 diffraction spots, each of which corresponds to a Fourier component

(structure factor) of the electron density within the unit cell of the crystal. By recording diffraction images over a range of crystal orientations, a nearly complete set of structure factors is experimentally determined. The inverse Fourier transform of the structure factors reconstructs the electron density within the unit cell of the crystal (11). Because the level of photolysis is incomplete (~23%), the measured structure factors have contributions from both photolyzed and unphotolyzed states. To generate electron density maps of the photolyzed state, we extrapolate the partially photolyzed structure factors to complete photolysis. High-resolution electron density maps of L29F MbCO before and after photolysis are shown in Fig. 4; color contrast is used to highlight the structural differences (12). This color-coded presentation of the experi-

mentally determined electron density requires an estimate of the level of photolysis; however, this estimate need not be precise, as minor variations in the degree of photolysis alter only the absolute magnitude of the motion, not the relative magnitude nor its direction. Because each structure is determined from data collected before and after photolysis in an interleaved fashion on the same crystal, the photolysis-induced structural differences are revealed with high precision, despite the relatively low level of photolysis.

Correlated displacements of the heme, the protein backbone, and other side chains are evident throughout the protein at 100 ps (see Fig. 4A), which is consistent with spectroscopic studies that report significant conformational relaxation by that time (13, 14). The heme tilts toward the distal residues, with a hinge point located near the propionate side chains. The driving force for this motion resides in a photolysis-induced displacement of the heme iron: Atomic resolution structures of Mb show the iron in the plane of the heme in MbCO but displaced 0.30 Å (15) or 0.36 Å (16) in the proximal direction in Mb. This displacement generates downward pressure on the His⁹³ and upward pressure on the heme. The strain is relieved largely by the tilt of the heme and, to a lesser extent, by displacement of the proximal histidine. As the heme tilts, it drags with it the side chains Leu¹⁰⁴ and Ile¹⁰⁷ and the G helix to which they are attached. The largest amplitude motion occurs near the binding site and involves displacement of CO, Phe²⁹, and His⁶⁴. The displacement of these side chains is much more dramatic than the static structural differences between deoxy Mb (Protein Data Bank 1MOA) and MbCO (Protein Data Bank 2SPL). To accommodate the ~2 Å displacement of the docked CO (labeled 1 in Fig. 4), the Phe²⁹ twists and moves upward, pushing His⁶⁴ away from the ligand-binding site, a direction of motion nearly opposite that observed on longer nanosecond time scales or in the equilibrium state with no bound ligand (15, 16). Concomitant with the ejection of CO from the primary docking site, the Phe²⁹ and His⁶⁴ residues relax toward their deoxy Mb configuration. Apparently, the strain energy retained by these side chains accelerates the departure of docked CO 1000 times compared with the rate of CO escape from wild-type Mb; this strain energy corresponds to an Arrhenius energetic bias of 16 kJ mol⁻¹ at 283 K (about half the wild-type activation energy barrier for ligand departure from the primary docking site).

As CO escaped from site 1, we observed electron density appearing in sites 2 and 3. Site 3 corresponds to the so-called Xe4 site, one of several internal hydrophobic cavities found to harbor Xe under pressure (17). The CO residence time in the Xe4 site is rather

Fig. 2. Sample geometry used to acquire picosecond time-resolved x-ray diffraction data. The crystal was photolyzed by a laser pulse and then probed by a time-delayed x-ray pulse, whose diffraction pattern was recorded on a charge-coupled device (CCD) area detector. A custom fixture supported the MbCO crystal (0.2 by 0.2 by 0.2 mm) in a sealed capillary at a 45° angle relative to the goniometer rotation axis. The laser beam was directed along the rotation axis with the intersection of the laser and x-ray beams centered 50 μm inside the pump-illuminated face of the crystal. The laser pulse was focused to a 0.2 by 0.12 mm spot (full width at half maximum, FWHM), which modestly overfilled the volume probed by the 0.1 by 0.1 mm x-ray beam. A 10°C cooling stream from an Oxford Cryostream extracted excess heat from the crystal, permitting laser photolysis at 3.3 Hz with no ill thermal effects.

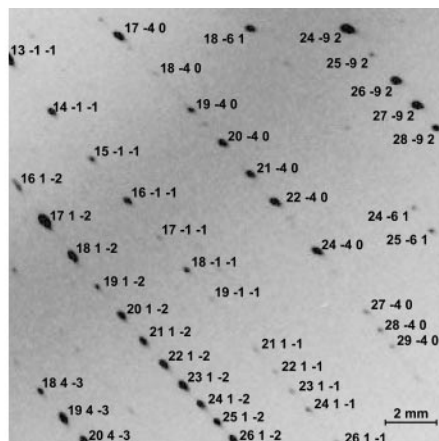
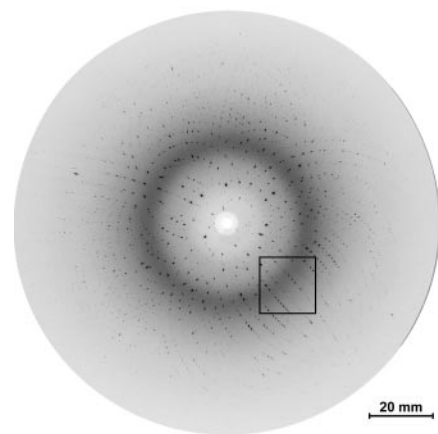
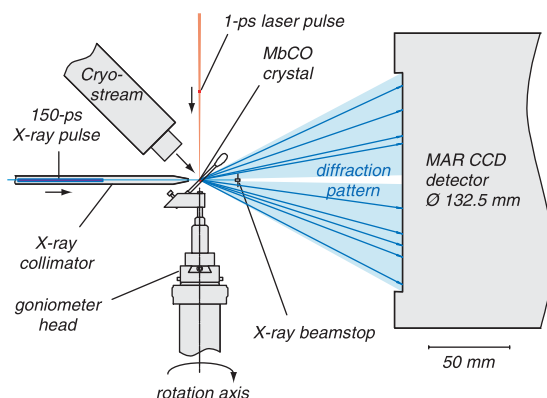
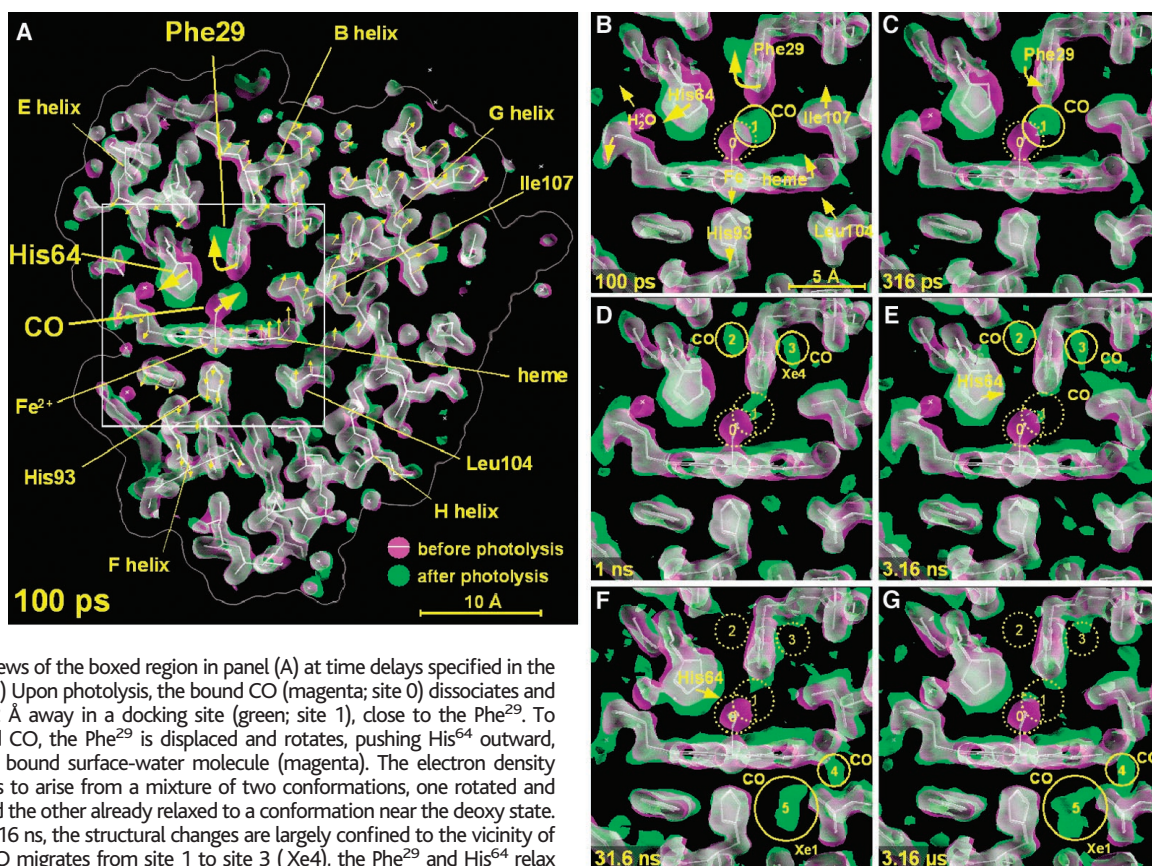


Fig. 3. One of 155 time-resolved Laue diffraction patterns recorded from a single, low-mosaicity P6 crystal of L29F MbCO. This image contains about 3000 diffraction spots, each of which corresponds to a Bragg reflection from a set of crystallographic planes. Many spots are simultaneously excited by the undulator radiation, whose useful intensity range spans about 0.72 to 1.24 Å. Only a small fraction of these spots would appear when probed with monochromatic x-ray radiation. The enlarged view identifies Miller indices associated with the crystallographic planes that generated the corresponding Bragg reflections. This 10-s exposure, acquired midway through the series, represents the cumulative diffracted intensity from 32 x-ray pulses with the pump-probe delay set to 100 ps.

REPORTS

Fig. 4. (A) Experimentally determined electron densities within a 6.5-Å-thick slice through the myoglobin molecule before (magenta) and 100 ps after (green) photolysis. Where these densities overlap, they blend to white. The white-stick model corresponds to the unphotolyzed structure and is included to guide the eye. The direction of molecular motion follows the magenta-to-green color gradient. Three large-scale displacements near the CO-binding site (large arrows) are accompanied by more subtle correlated rearrangements throughout the entire protein (small arrows; not drawn to scale). (B to G) Enlarged views of the boxed region in panel (A) at time delays specified in the lower left of each panel. (B) Upon photolysis, the bound CO (magenta; site 0) dissociates and becomes trapped about 2 Å away in a docking site (green; site 1), close to the Phe²⁹. To accommodate the docked CO, the Phe²⁹ is displaced and rotates, pushing His⁶⁴ outward, which in turn dislodges a bound surface-water molecule (magenta). The electron density surrounding Phe²⁹ appears to arise from a mixture of two conformations, one rotated and displaced toward His⁶⁴ and the other already relaxed to a conformation near the deoxy state. (C to E) From 316 ps to 3.16 ns, the structural changes are largely confined to the vicinity of the binding site. As the CO migrates from site 1 to site 3 (Xe4), the Phe²⁹ and His⁶⁴ relax toward their deoxy conformations, which are similar to their unphotolyzed states. (F and G) Structures acquired after nanosecond photolysis of a second protein crystal. By 31.6 ns, CO has migrated to sites 4 and 5, where it remains trapped for microseconds. The magenta and green maps were contoured at the same absolute level (1.5 σ of the unphotolyzed density) using O 7.0, author A. Jones. [See Movie S1 to view the time-dependent electron density changes.]



short-lived: It departs by 32 ns and migrates around the heme to sites 4 and 5 (Xe1), where it persists for microseconds. Ligand migration from Xe4 to Xe1 presumably requires a protein fluctuation to permit passage around the heme, an event that occurs within a few tens of nanoseconds. The Xe4 intermediate observed here has not been seen in wild-type Mb, where the rate of CO escape from the primary docking site is slow compared with the rate of CO migration from Xe4 to Xe1. Therefore, L29F-induced destabilization of CO in the primary docking site made it possible to characterize the protein dynamics associated with CO passage around the heme. Because CO remains sequestered in hydrophobic cavities at 3.16 μ s (see Fig. 4G), time-resolved structures at longer times will be needed to identify pathways for ligand escape into the surrounding solvent.

In earlier work, the Xe1 site was shown to harbor CO indirectly through mutagenesis and Xe studies (18), as well as directly by pioneering nanosecond time-resolved crystallographic studies (19). In addition, cryocrystallography studies of photolyzed L29W (20) and L29Q MbCO (21) found CO in the Xe4 site, whereas studies of wild-type horse MbCO found CO in the

Xe1 site (22). When photolysis of L29W MbCO was followed by thermal cycling above the Mb glass transition temperature, CO was found to migrate from Xe4 to Xe1 (20), as observed here in real time. The highly strained intermediate observed in our 100-ps snapshot has not yet been trapped under cryogenic conditions, and it is unlikely that it could be. Moreover, cryocrystallography cannot assess protein dynamics under physiologically relevant conditions where thermally driven conformational fluctuations lead to rapid interconversion among conformational substates (23). Nevertheless, the method of cryocrystallography, with its higher spatial resolution, is a useful complement to time-resolved crystallographic methods.

The static structures of thousands of proteins are known, yet there is no single protein whose function is fully understood at an atomic and deterministic level. In this time-resolved study, the interplay between a protein and a docked ligand is clearly revealed, with picosecond correlated side-chain motion providing a structural explanation for the ultrafast departure of docked CO. By extending the time-resolution of crystallography into a time domain readily accessible to molecular

dynamics simulations, we pave the way for exploring functionally important structure transitions both theoretically and experimentally. Whereas the time resolution of macromolecular crystallography at the ESRF is, for all practical purposes, currently limited by the x-ray pulse duration to \sim 100 ps, the chemical time scale will be accessible to x-ray free electron lasers, which promise to deliver intense x-ray pulses shorter than 100 fs (24).

References and Notes

- As of July 2002, more than 12,000 protein structures have been deposited into the Protein Data Bank, of which nearly 3300 are characterized as enzymes [H. M. Berman *et al.*, *Nucleic Acids Res.* **28**, 235 (2000)].
- R. H. Austin, K. W. Beeson, L. Eisenstein, H. Frauenfelder, I. C. Gunsalus, *Biochemistry* **14**, 5355 (1975).
- A. Ansari, C. M. Jones, E. R. Henry, J. Hofrichter, W. A. Eaton, *Biochemistry* **33**, 5128 (1994).
- T. A. Jackson, M. Lim, P. A. Anfinrud, *Chem. Phys.* **180**, 131 (1994).
- X. Ye, A. Demidov, P. M. Champion, *J. Am. Chem. Soc.* **124**, 5914 (2002).
- M. H. Lim, T. A. Jackson, P. A. Anfinrud, *J. Chem. Phys.* **102**, 4355 (1995).
- D. Vitkup, G. A. Petsko, M. Karplus, *Nature Struct. Biol.* **4**, 202 (1997).
- I. Schlichting, J. Berendzen, G. N. Phillips Jr., R. M. Sweet, *Nature* **371**, 808 (1994).
- T. Y. Teng, V. Srajer, K. Moffat, *Nature Struct. Biol.* **1**, 701 (1994).

10. T. E. Carver *et al.*, *J. Biol. Chem.* **1992**, 14443 (1992).
 11. Materials and methods are available as supporting material on Science Online.
 12. We believe that the extrapolated electron density maps presented here are more informative than difference electron density maps. With difference maps, only those structural changes whose difference density rises above a specified threshold (contour level) are observable. Moreover, those features are only rarely centered on the atoms that move, which makes it more difficult to visualize the atomic motion.
 13. M. Lim, T. A. Jackson, P. A. Anfinsen, *Proc. Natl. Acad. Sci. U.S.A.* **90**, 5801 (1993).
 14. G. D. Goodno, A. Astinov, R. J. D. Miller, *J. Phys. Chem. A* **103**, 10630 (1999).
 15. G. S. Kachalova, A. N. Popov, H. D. Bartunik, *Science* **284**, 473 (1999).
 16. J. Vojtechovsky, K. Chu, J. Berendzen, R. M. Sweet, I. Schlichting, *Biophys. J.* **77**, 2153 (1999).
 17. R. F. Tilton Jr., I. D. Kuntz Jr., G. A. Petsko, *Biochemistry* **23**, 2849 (1984).
 18. E. E. Scott, Q. H. Gibson, J. S. Olson, *J. Biol. Chem.* **276**, 5177 (2001).
 19. V. Srajer *et al.*, *Biochemistry* **40**, 13802 (2001).
 20. A. Ostermann, R. Waschipyk, F. G. Parak, G. U. Nienhaus, *Nature* **404**, 205 (2000).
 21. M. Brunori *et al.*, *Proc. Natl. Acad. Sci. U.S.A.* **97**, 2058 (2000).
 22. K. Chu *et al.*, *Nature* **403**, 921 (2000).
 23. H. Frauenfelder, G. U. Nienhaus, J. B. Johnson, *Ber. Bunsen-Ges. Phys. Chem.* **95**, 272 (1991).
 24. A. Cho, *Science* **296**, 1008 (2002).
 25. We thank W. Eaton and G. Hummer for helpful comments, and D. Bourgeois for sharing his expertise in the analysis of Laue diffraction data. We are grateful to K. Moffat and V. Šrajer for their assistance during our early struggles to realize picosecond x-ray crystallography. This work was supported by grants

from the Robert A. Welch Foundation (C-612), the NIH (HL47020 and GM35649), and the W. M. Keck Center for Computational Biology to J.O.; by grants from the Robert A. Welch Foundation (C-1142) and the NIH (AR40252) to G.P.; and by grants from the Korea Science and Engineering Foundation, through the Center for Integrated Molecular Systems (POSTECH), to M.L.

Supporting Online Material

www.sciencemag.org/cgi/content/full/300/5627/1944/DC1

Materials and Methods

Table S1

Movie S1

References

26 September 2002; accepted 14 May 2003

Kin Selection in Cooperative Alliances of Carrion Crows

Vittorio Baglione,^{1*} Daniela Canestrari,¹ José M. Marcos,² Jan Ekman¹

In most cooperative vertebrates, delayed natal dispersal is the mechanism that leads to the formation of kin societies. Under this condition, the possibility that kin-based cooperative breeding is an unselected consequence of dispersal patterns can never be ruled out because helpers can only help their relatives. Here we show that a population of carrion crows (*Corvus corone corone*) fully fits the central prediction of kin selection theory that cooperative breeding should arise among relatives. On their territory, resident breeders are aided not only by nonbreeding retained offspring but also by immigrants (mainly males), with whom they share matings. Philopatry cannot account, however, for the high degree of genetic relatedness found between breeders and immigrants of the same sex that cooperate at a nest, indicating that crows actively choose to breed cooperatively with their relatives.

Kin selection operates whenever relatives interact (1), but its role in the evolution of social behavior has recently been questioned. Despite the fact that the majority of vertebrate cooperative species live in kin groups, high relatedness among group members represents only weak evidence of the importance of kin selection in shaping the social system (2–5). In fact, kin-based cooperative breeding might be an unselected consequence of dispersal patterns. Helpers in vertebrates are typically offspring that remain with their parents on their natal territory (6) and thus do not have the option of choosing between helping relatives or helping unrelated individuals (2). In some societies, individuals disperse from the natal territory in related coalitions [such as the acorn woodpecker *Melanerpes formicivorus* (7)], leading again

to kin-directed cooperation. On the other hand, cooperative polyandry (8) among nonrelatives is widespread among vertebrates (9) and proves that cooperative breeding can arise in the absence of indirect fitness benefits.

In a cooperatively breeding population of carrion crows (*Corvus corone corone*) in northern Spain, helpers are either nondispersing offspring that assist their parents on the natal territory or immigrants (mostly males) that associate with a territorial pair, forming stable groups that live year-round in all-pur-

pose territories (10–12). Breeding units are therefore either unassisted pairs, pairs with nondispersing 1- or 2-year-old offspring, pairs with immigrants, or pairs with both immigrants and nondispersing offspring. Male immigrants often share matings with the resident breeders (67% of groups containing sexually mature immigrants) (11).

We have been banding all crow nestlings reared in a 45-km² study area at La Sobarriba (in northern Spain, 42°N, 5°W) since 1995. Because juveniles delay natal dispersal for up to 2 years but never inherit the natal territory (10), we have been able to determine for every individual since 1997 whether it was currently living on its natal territory or not. In 1999 and 2000, we captured 61 free-flying crows (10), collecting information on 21 social groups, 13 of which contained one or two immigrants. The aim of this study was to investigate pairwise relatedness among same-sex immigrants and resident breeders (17 dyads) that associated on a territory (13). Relatedness estimates were based on allele frequencies at six polymorphic microsatellite loci (14). Relatedness between immigrants and residents was compared to the average degree of relatedness among individuals in the population, calculated on the entire sample of genotyped crows [137 individuals captured in the study area, 9316 pairwise estimates of relatedness (*r*) (13).

Same-sex immigrant and resident crows showed a high degree of relatedness (mean

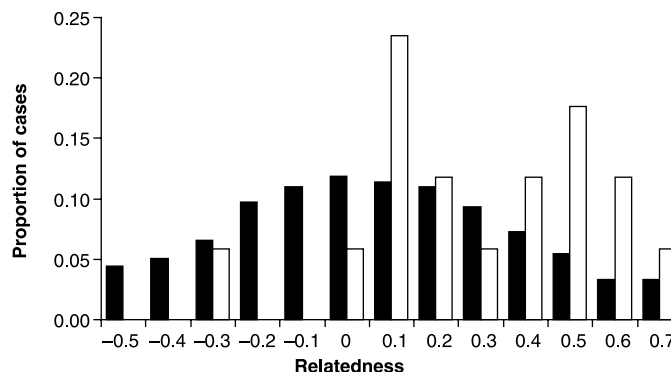


Fig. 1. Distribution of pairwise *r* estimates in the population (solid bars) and in the sample of same-sex immigrant and resident crows cooperating on a territory (open bars).

¹Population Biology/Evolutionary Biology Centre, Uppsala University, Norbyvägen 18D, SE-752 36, Uppsala, Sweden. ²Physiology and Animal Biology, University of Sevilla, Avenida Reina Mercedes 6, 41071 Sevilla, Spain.

*To whom correspondence should be addressed. E-mail: vittorio.baglione@ebc.uu.se